HHS Public Access

Author manuscript

ACS Sens. Author manuscript; available in PMC 2024 October 27.

Published in final edited form as:

ACS Sens. 2023 October 27; 8(10): 3845–3854. doi:10.1021/acssensors.3c01369.

Ultra-Low-Cost Disposable Handheld Clinical-scale Propane Gas Hyperpolarizer for Pulmonary MRI Sensing

Nuwandi M. Ariyasingha[a], **Anna Samoilenko**[a], **Jonathan R. Birchall**[a], **Md Raduanul H. Chowdhury**[a], **Oleg G. Salnikov**[b], **Larisa M. Kovtunova**[b,c], **Valerii I. Bukhtiyarov**[c], **David C. Zhu**[d], **Chunqi Qian**[d], **Michael Bradley**[e], **Juri G. Gelovani**[a,f], **Igor V. Koptyug**[b], **Boyd M. Goodson**[g], **Eduard Y. Chekmenev**[a,h]

[a]Department of Chemistry, Integrative Bio-sciences (Ibio), Karmanos Cancer Institute (KCI), Wayne State University, Detroit, Michigan 48202, United States

[b]International Tomography Center SB RAS, 3A Institutskaya st., Novosibirsk 630090, Russia

[c]Boreskov Institute of Catalysis SB RAS, 5 Acad. Lavrentiev pr., Novosibirsk 630090, Russia

[d]Department of Radiology, Michigan State University, East Lansing, MI 48824, USA

[e]Division of Laboratory Animal Resources, Wayne State University, Detroit, Michigan 48202, United States

[f]United Arab Emirates University, Al Ain, United Arab Emirates

[g]School of Chemical & Biomolecular Sciences, Materials Technology Center, Southern Illinois University, Carbondale, IL 62901, USA

[h]Russian Academy of Sciences, 119991 Moscow, Russia

Abstract

Hyperpolarized MRI (magnetic resonance imaging) contrast agents are revolutionizing the field of biomedical imaging. Hyperpolarized Xe-129 was recently FDA approved as an inhalable MRI contrast agent for functional lung imaging sensing. Despite success in research settings, modern Xe-129 hyperpolarizers are expensive (up to $1M), large, and complex to site and operate. Moreover, Xe-129 sensing requires specialized MRI hardware that is not commonly available on clinical MRI scanners. Here, we demonstrate that *proton*-hyperpolarized propane gas can be produced on demand using a disposable, handheld, clinical-scale hyperpolarizer via parahydrogen-induced polarization, which relies on parahydrogen as a source of hyperpolarization. The device consists of a heterogeneous catalytic reactor connected to a gas mixture storage can containing pressurized hyperpolarization precursors: propylene and parahydrogen (10 bar total pressure). Once the built-in flow valve of the storage can is actuated, the precursors are ejected from the can into a reactor, and a stream of hyperpolarized propane gas is ejected from the reactor. Robust operation of the device is demonstrated for producing proton sensing polarization

chekmenevlab@gmail.com .

ASSOCIATED CONTENT

Supporting Information. Additional experimental details, materials, and methods, including NMR spectra, time-resolved NMR spectroscopy, experimental setup schematic, MRI images, annotated MATLAB code. PDF. This material is available free of charge via the Internet at http://pubs.acs.org.

of 1.2% in a wide range of operational pressures and gas flow rates. We demonstrate that propylene:parahydrogen gas mixture can retain potency for days in the storage can with mono-exponential decay time constant of 6.0 ± 0.5 days, which is limited by the lifetime of the parahydrogen singlet spin state in the storage container. The utility of the produced sensing agent is demonstrated for phantom imaging on a 3 T clinical MRI scanner located 100 miles from the agent/device preparation site, and also for ventilation imaging of excised pig lungs using a 0.35 T clinical MRI scanner. The cost of the device components is less than $35, which we envision can be reduced to less than $5 for mass-scale production. The hyperpolarizer device can be re-used, recycled, or disposed.

Graphical Abstract

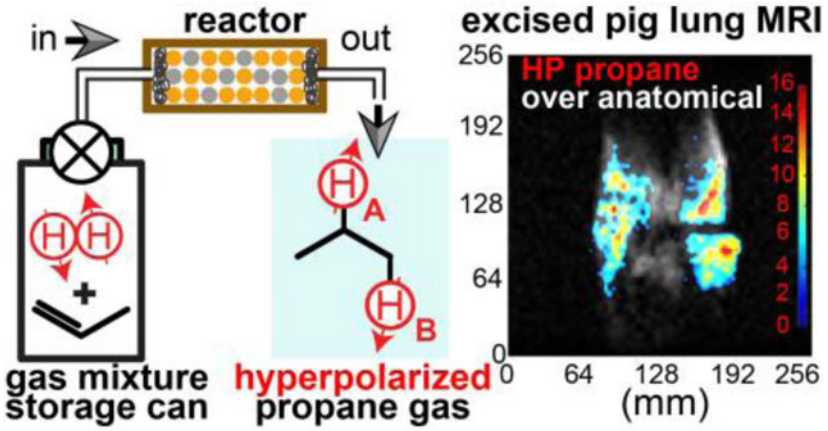

Keywords

MRI; hyperpolarization; imaging agents; NMR spectroscopy; parahydrogen; propane

Biomedical imaging is an important tool in the study of human anatomy and physiology for disease diagnosis, progression monitoring, and characterizing response to treatment. In particular, MRI imaging is widely used due to its non-invasive nature for obtaining structural, functional, and dynamical information in subject tissues of interest. MRI employs NMR (nuclear magnetic resonance), which is regarded as a low-sensitivity spectroscopic technique[1–2] due to its inherently low degree of nuclear spin alignment with respect to the applied magnetic field, or spin polarization (*P*); for example, the most-sensitive stable nucleus, proton (^{1}H), is polarized to only 1×10^{-5} at 3 T and room temperature. To mitigate this NMR sensitivity limitation, conventional MRI is performed with highly abundant water protons, *ca.* 10^2 M. Alternatively, a substantial *P* enhancement by 4–6 orders of magnitude can be transiently created via NMR hyperpolarization techniques.[3–8] As a result of this massive *P* boost, it becomes possible to sense low-concentration hyperpolarized (HP) biomolecules and exogenous contrast agents.[2, 9] Moreover, NMR hyperpolarization also enables the potential use of HP gases as inhalable contrast agents to image structure of the lungs and pulmonary function.[3, 7, 9–11]

Hyperpolarization also allows rapid image acquisition because it obviates spin magnetization recovery in imaging sequences that is often otherwise required in conventional MRI. HP noble gases (*e.g.*, ^{129}Xe and ^{3}He) can be prepared in large quantities for clinical studies.[9, 12–14] These contrast agents can be inhaled, and a functional pulmonary 3D image can be recorded on a single patient breath hold (~3–10 seconds).[3, 9] While both batch- and continuous-production modes have been demonstrated for hyperpolarization of noble gases,[11] these hyperpolarization methods usually require the presence of complex on-site hyperpolarizer instrumentation and infrastructure.[15–20] Once the hyperpolarizer dispenses the agent, its HP state decays to thermal equilibrium. Due to the short-lived, non-replenishable characteristic of the HP state, the long-range transportation of these HP contrast agents remains challenging.[21] As a result, production of HP noble gases is established on site, which creates additional logistics challenges including the local requirement of expertise in production and imaging of HP media.[17]

The leading inhalable HP contrast is ^{129}Xe,[9] which is hyperpolarized via Spin Exchanged Optical Pumping (SEOP);[17] near-unity polarization is possible via SEOP.[16, 19, 22] HP ^{129}Xe is extensively studied for a wide range of *in vivo* applications, including pulmonary imaging.[9, 11, 23] Indeed, the use of HP ^{129}Xe for pulmonary function imaging was approved by the FDA in 2022. Despite major successes of HP ^{129}Xe in research settings to help to diagnose a wide range of lung conditions, the clinical translation of this HP contrast agent and its production technology faces two key translation barriers.[1, 24–25] First, in addition to the instrumentation complexity discussed above, SEOP hyperpolarizers are also expensive, *e.g.*, up to $1M *ca.* 2022.[3] Second, conventional MRI scanners can only image protons, which resonate at a frequency ~3.6 times higher than that of ^{129}Xe— placing the ^{129}Xe resonance far below the narrow tuning range of MRI scanner electronics. As a result, an upgrade of a clinical MRI scanner is required to add broadband multi-nuclear capability to enable ^{129}Xe scans. These upgrades are complex, costly ($0.3-$0.5M), and limited to a selected vendor's platforms. Taken together, these issues comprise substantial roadblocks for a widespread clinical use of the HP ^{129}Xe gas contrast agent for pulmonary sensing applications.

Proton-hyperpolarized gases have shown promise for MRI applications.[26–29] Although the lifetime of their HP state is short (with T_1 on the order of 1–1.2 s)[21, 30] at physiologically relevant conditions, the discovery of long-lived HP states has rekindled interest in the utility of proton-hyperpolarized gases for bio-imaging sensing applications because the lifetime of the HP state was increased approximately by a factor of three.[21, 31] We have previously demonstrated the feasibility of production of *proton*-hyperpolarized propane gas on a clinical scale: 0.3-liter bolus of HP gas was produced in 2 seconds.[32] The production of HP propane was enabled by heterogeneous parahydrogen induced polarization (HET-PHIP),[33–34] where parahydrogen was reacted with propylene in a packed bed of heterogeneous catalyst (1% Rh/TiO_2[33]). In PHIP, parahydrogen (p-H_2) acts as a source of hyperpolarization.[34–36] p-H_2 is produced using cryogenic equipment and dispensed into high-pressure aluminum cylinders, where it can be stored for weeks without significant loss of p-H_2 fraction.[37–38]

Here, we report on the design and validation of an ultra-low-cost disposable hand-held propane gas hyperpolarizer. This device employs an aluminum can typically used for consumer spray applications. The can is filled with a pressurized mixture of p-H_2 and propylene gases via a built-in plastic high-flow valve. The output of the can is connected to a HET-PHIP reactor. Once the valve is manually actuated, the gas mixture stream flows through the reactor, where the gases are chemically converted to proton-hyperpolarized propane gas, which can be employed for sensing of void spaces. The continuous flow of the gas provided by the device enables the production of a stream of HP propane gas free from catalyst, which is retained in the heterogeneous catalyst bed of the reactor. We demonstrate the robustness of the hyperpolarizer operation to produce ^{1}H polarization (P_H) of 1.2% with respect to a wide operational range of temperatures, pressures, and gas flow rates. Moreover, we also show that the compressed p-H_2-propylene gas mixture can be stored for days without substantial loss of potency to produce HP propane gas. As a result, it becomes possible to transport this device over a long distance—here, we show the feasibility of transporting the hyperpolarizer over 100 miles to acquire HP propane gas MR images in a phantom at 3 T with high temporal and spatial resolution. Moreover, we also demonstrate the feasibility of employing this hyperpolarizer for production of HP propane gas for ventilation imaging in excised pig lungs. The cost of all components and reagents to make this device is less than $35, with over 80% of the cost associated with connectors. We anticipate that a commercialized prototype can be made with less than $5 for the cost of all components, which bodes well for future clinical translation of proton-hyperpolarized gas contrast agents—including propane sensor gas employed here.

MATERIALS AND METHODS

p-H_2 decay in disposable aluminum cans.

Figure 1 summarizes measurements of the back-conversion of p-H_2 to normal H_2 in storage cans of two different sizes: ~0.12 standard liters (type 1) and ~0.25 standard liters (type 2). Commercial cans were thoroughly cleaned first by flushing with argon gas followed by gas evacuation with a vacuum pump. Finally, the cans were also flushed several times with p-H_2 to remove any trapped air. For these tests, ParaSun p-H_2 generator was employed yielding ~89% para- fraction.[37] The overall experimental setup is shown in Figure 1a. For the type 1 can, a sample of freshly prepared p-H_2 gas was filled into a storage can (Boost Oxygen) via ¼-inch outer diameter (OD) Teflon tubing to a total p-H_2 pressure of 13 bar. This Teflon tubing (placed over the can actuator) connects the p-H_2 temporary storage tank with the aluminum can. For the type 2 can, the setup was overall the same, except that the connection with the can was established via cleaned copper tubing (3/16-inch OD) inserted inside the actuator. Unlike the type 1 can, the type 2 can employs a built-in fast-flow valve capable of maximum gas flow rate in excess of 0.5 standard liters per second (sLs) or 30 standard liters per minute (sLm). Once a can was filled with p-H_2 gas, the p-H_2 gas was stored inside the cans for a variable period of time ranging from a few minutes to nearly 8 days, with the overall rationale of testing the mixture for the residual p-H_2 fraction, which decays with time. ^{1}H NMR spectra were collected by releasing p-H_2 gas from the aluminum storage can by pressing down on the actuator to release the gas into the NMR tube setup, which was placed inside the magnet of a 1.4 T benchtop NMR spectrometer

(Nanalysis NMR Pro 60) at an overpressure of 100 psi. After 3–4 seconds of continuous gas flow, the flow was terminated by releasing the pressure applied to the actuator and by manually closing gas inlet valve. Once the NMR tube was filled, the stopped gas was analyzed by NMR spectroscopy as described previously.[38] Examples of NMR spectra are shown in Figures 1b and 1c. For NMR acquisition, we employed 90-degree radiofrequency (RF) excitation pulses with recovery time of 3 seconds and 64 averages. The recorded NMR spectra reveal the presence of o-H_2 only because p-H_2 is NMR-inactive. The spectral intensities were employed to compute o-H_2 and p-H_2 fractions in the samples as described in detail in Supporting Information (SI). The additional bypass valve of the setup is present to ensure venting of the lines if needed. The determined residual p-H_2 fraction was plotted as a function of storage time in type 1 and type 2 cans (Figure 1d and Figure 1e, respectively). The trend lines were fit using mono-exponential curves, yielding decay constants T_S of p-H_2 back-conversion to normal H_2.

The gas flow rate in the setup shown in Figure 2a was not controlled, and the actual flow rate was measured by water displacement of the exiting reacted gas via the safety valve (~7.5 sLm). The peak intensities of H_A and H_B resonances recorded during the pseudo-2D pulse-sequence dynamic run are shown in Figure 2f. The intensity decay was fit with a mono-exponential curve (Figure S2), yielding effective T_1 decay values. For the p-H_2:propylene mixture potency duration study, the pressurized storage can (type 2) was stored for a variable period of time before performing the PHIP experiment, and the maximum intensity of HP propane was plotted versus time, Figure 2g.

In a few studies requiring the precise control of the flow rate, a modified setup employing a mass-flow controller was employed, Figure S3 (see SI for more details).

HP propane MRI studies with phantoms at 3 T.

For all 3 T MRI studies, type 2 storage cans were filled with the 1:1 mixture of p-H_2:propylene gases as described above. The cans were transported approximately 100 miles from the filling site to the imaging site, and MRI studies were performed approximately 4–7 hours after the cans were filled with the compressed gas mixture. A pressurized can and a reactor were placed on a patient bed, while the phantom was placed inside the wrist RF coil of a 3 T GE Healthcare MRI scanner (Signa HDx, GE Healthcare, Waukesha, WI). Slice-selective 2D gradient echo imaging (GRE) and multi-slice 2D echo-planar imaging (EPI) sequences were employed for visualization of the HP propane gas and thermally-polarized reference phantom consisting of HPLC-grade water doped with 5 mM $CuSO_4$. Each imaging sequence was initiated before gas injection in the phantom, and repeated 32 or more times to capture the HP gas delivery into a phantom followed by HP gas decay due to RF excitation and T_1 decay. See SI for imaging sequence details.

HP propane MRI studies in excised pig lungs at 0.35 T.

All excised pig lungs were acquired from unrelated, IACUC approved studies at Wayne State University. For all 0.35 T MRI studies, type 2 storage cans were filled on site with the 1:1 mixture of p-H_2:propylene gases as described above. All MRI studies were performed within 30 mins after the cans were filled with the compressed gas mixture. A freshly

excised pig lungs (containing both lungs and trachea) was connected to ¼" ID Tygon tubing for HP propane gas injection (rubber band was also employed to compress trachea wall against Tygon tubing to prevent gas leakage). The following imaging parameters were employed: spectral width (SW) of 10.42 kHz, slice thickness of 5 cm, field of view (FOV) = 25.6×25.6 cm^2, imaging matrix of 64×64. 32 repeats of this scan were programmed in a loop fashion with acquisition time of 0.94 s for each individual 2D image (30-s total run time). Approximately 5–6 seconds after the start of the imaging experiment, the HP propane gas was injected in the lungs with injection lasting approximately 5–6 seconds, with an estimated injected volume of 0.7 sL (and estimated flow rate of 0.12 sLs). After the completion of the gas injection, the 1/8" Teflon tubing line was disconnected from the hyperpolarizer, and capped to prevent gas back flow from the lungs into the reactor. The images were acquired in axial and coronal projection with otherwise identical imaging parameters. Control runs with injection of nitrogen gas were performed with similar injection rate and injection volume (see SI for details). To enhance the visual clarity of the images, all of the images were interpolated to 256×256 with effective 1×1 mm^2 in-plane interpolated resolution.

RESULTS AND DISCUSSION

Hyperpolarized propane spectroscopy and enhancement quantification.

Polarization of each set of positively and negatively enhanced H_A and H_B NMR lines of HP propane was assessed in the stopped HP propane gas, which was trapped in the detection volume of the 1.4 T NMR spectrometer by closing the reactor inlet and outlet valves, Figure 2d. (note that fast-flowing HP propane exhibits severe line broadening, Figure 2c). In our approach, we recorded 64 1D spectra in a pseudo-2D fashion with repetition time of 0.5 s. The intensities of HP propane resonances H_A and H_B were plotted as a function of time, Figure 2f. Because the valve closing and the NMR acquisition are not time-synchronized, it follows that as much as 0.5 s may have passed before recording of the first NMR spectrum. P_H decays with a time constant T_1 of 2.9–3.1 s (Figure 2f), which is evident from the decay of the HP signal of the stopped propane gas in Figure S2.[21] Due to this uncertainty and the associated polarization decay, the presented method is susceptible to run-to-run signal variability. Moreover, the measured P_H value represents a lower estimate as the polarization may have experienced some decay during the time interval before the application of the first RF pulse. Despite these limitations, signal enhancement values in excess of 2500-fold were observed, Figure 2, corresponding to P_H of over 1.2% for H_A and H_B. These P_H and T_1 values are in overall agreement with previous relaxation studies.[21, 32] The chemical conversion of propylene was near 100% as no traces of propylene gas were detected in thermally polarized spectra at 7.5 sLm flow rate, Figure S1. Although the P_H levels of HP propane gas are substantially lower than those typically obtained for HP ^{129}Xe gas (*i.e.*, typically in excess of 20%),[11] we note that each HP propane molecule carries double the magnetization load (two HP protons versus one HP ^{129}Xe nucleus). Moreover, each proton is typically 13 times more sensitive than HP ^{129}Xe at the same nominal polarization due to 3.6-times greater gyromagnetic ratio (one gamma for greater magnetic moment multiplied by one more gamma for higher detection frequency).[39] Furthermore, protons have nearly 100% natural abundance compared to 26% natural abundance of ^{129}Xe. These compounding

factors make 1%-hyperpolarized propane equivalent to 100%-hyperpolarized ^{129}Xe at natural abundance or equivalent to 32%-hyperpolarized ^{129}Xe at an 80% enrichment level. Furthermore, this sensitivity analysis does not factor in the fact that RF coils for detecting proton MRI are usually highly optimized by vendors in the clinical practice, which may additionally favor HP propane imaging sensitivity.

Hyperpolarizer reactor robustness.

While most of the studies reported here were performed with a 7.5 sLm HP propane flow rate, we have additionally performed a series of studies using a modified setup (Figure S3) to investigate the reactor robustness with respect to the pressure, gas flow rate, and gas flow duration by adding an additional control element of a mass flow controller or a needle valve. This modified setup shown in Figure S3 also employed p-H_2 with variable para- fraction between 50% to 90%. The hyperpolarizer reactor operation robustness was evaluated in several ways. First, we have modified our pseudo-2D experiments (shown in Figure 3a), and have performed a series of additional valve openings/closings, effectively resulting in the inflow of fresh HP propane gas in the detection region of the NMR spectrometer, Figure 3b. In this representative dynamic run, signal enhancement ε_H of ~1600-fold was repeatedly achieved five times sequentially, clearly indicating good reproducibility. Additionally, Figure 3b indicates the possibility of HP propane gas production effectively on demand.

The reactor has shown overall robust performance with relatively small variation of signal enhancement of HP propane gas (estimated at ±20%) with respect to pressure range studied (4.4–7.8 bar, gas flow rate of 0.8 sLm) for the gas mixtures containing 1:1 and 1:4 propylene:p-H_2 composition ratios, Figure 3c and Figure 3d respectively.

HP propane signal enhancements exhibited relatively low dependence on the gas flow rate in the 0.4–2.8 sLm range studied, Figure 3e (for the variable flow-rate experiments, the mass flow controller was replaced by a needle valve). The variation of ε_H values was estimated to be ±10%, and the chemical conversion of propylene was near 100% at all flow rates studied.

In a separate set of experiments, we have varied the duration of the HP gas flow at 0.8 sLm flow rate before the flow was terminated, Figure 3f. Similarly to the data shown in Figure 3e, the variation of ε_H values was estimated to be ±10%, and the chemical conversion of propylene was near 100% at all flow duration timings studied, Figure 3f.

All-in-all, the hyperpolarizer reactor has demonstrated good robustness of operation with respect to a wide range of experimental parameters. The entire device consisting of the reactor, gas storage can with the gas mixture, and connecting tubing weights less than 200 g. The cost of all components is approximately $35 with the following breakdown: compression fittings ($28), titania (200 mg, less than $0.1), rhodium (2 mg, $3), copper particles (10 g, $1.5), copper and Teflon tubing ($1.5), propylene (2 g, $0.1), hydrogen gas (0.2 g, less than $0.1), and aluminum can ($1). We anticipate that future integration of the reactor using a purpose-built design can substantially reduce the cost of the mechanical components. Moreover, the mass-scale production is also envisioned to reduce the cost of rhodium-containing precursor and other consumables with the total production cost of less than $5.

Decay of p-H_2 in aluminum storage cans.

The p-H_2 decay due to para- to orthohydrogen conversion was found to occur with time constants T_S of 2.9 ± 0.6 and 6.4 ± 1.3 days at 13 bar in type 1 and type 2 cans, respectively (Figure 1d and Figure 1e). It should be noted that the type 2 can has approximately a two-times-greater inner diameter, and thus the collision rate of p-H_2 molecules with the container wall is expected to be doubled in a type 1 container compared to that for type 2 container. The fact that effective first-order rate constant of ortho/para-H_2 conversion in type 1 can is ~2 times greater than that in type 2 can suggests that the collision of p-H_2 gas with the container wall is the dominant channel of ortho/para conversion. Since the potency of the gas mixture to produce HP propane depends on the residual p-H_2 fraction at the time of the experiment,[6, 40] the p-H_2 lifetime studies in the gas mixtures with propylene were measured in a larger type 2 aluminum container using signal enhancement of produced HP propane as an observable (Figure 2g). The observed decay of potency of the propylene:p-H_2 gas mixture was found to have T_S of 6.0 ± 0.5 days at 10 bar total pressure. This T_S value is close to that in a can filled with pure H_2 and is sufficiently long for a short-term storage or transportation of propylene:p-H_2 gas mixtures for their utility in hyperpolarization studies. These T_S values are much shorter than the previously reported T_S value of 63.7 ± 8.3 days in substantially larger aluminum tanks,[41] likely because of the much smaller sizes of the aluminum storage containers employed here. Thus, we speculate that future improvement of storage can design can allow to extend the effective lifetime of propylene:p-H_2 gas mixtures and enable even longer storage and transportation time windows. The use of small storage cans is advantageous compared larger compressed gas aluminum tanks due to the low cost (< $1) and the possibility to dispose or recycle the storage can.

HP propane MRI studies with phantoms at 3 T.

The experimental setup employs a hollow plastic spherical phantom for filling with HP propane, Figure 4a, and the gas-mixture storage can connected directly to the reactor. The phantom sphere was placed inside the wrist RF coil of a 3 T MRI scanner (Signa HDx, GE Healthcare), whereas all other components (connected to the phantom via gas input and output Teflon tubing lines) were placed outside the MRI scanner because the safety valve (2.7 bar overpressure) and the storage can metal cup contain magnetic materials. The estimated gas flow rate was ~7.5 sLm. Since the scan time was less than a second, a series of looped scans was initiated shortly before the gas injection. After the HP propane gas injection for approximately 2 s, the flow valve was closed to prevent any HP gas back flow, and the HP propane gas was effectively stopped inside the imaging phantom.

The reader is reminded that HP propane molecule exhibits two resonances: H_A and H_B (with 180º phase shift) separated by 0.45 ppm (*i.e.*, 57 Hz at 3 T). As a result, MRI imaging of such HP species may exhibit several artifacts. First, partial signal cancellation (due to opposite phase of HP H_A and H_B resonances) may be possible due to low magnetic field homogeneity of the MRI scanner. Second, partial signal cancellation may also be possible between the adjacent pixels in a slice-selected imaging plane as well as between the neighboring slices.[42–44] Third, the presences of two resonances may lead to the additional “ghosting” (also called chemical shift) artifacts between the neighboring pixels in a slice-selected imaging plane as well as between the neighboring slices.[42–44]

A time series of high-resolution 2D GRE images with voxel size of 1×1×5 mm^3 acquired on a single injection of HP propane gas is shown in Figure 4b. Each image was acquired in 0.84 s with the maximum recorded signal to noise ratio (SNR(max)) of 38, which compares well to the SNR(max) of 179 on the corresponding image of thermally-polarized water phantom with similar dimensions, Figure 4b. The SNR of subsequent images decreases rapidly due to depolarizing effects of RF excitation pulses and T_1 decay. This pilot GRE image acquired using our disposable hand-held polarizer is important as it shows the feasibility of recording high-resolution HP propane gas images with mm-resolution using a clinical MRI scanner. Additional images from this series are also shown in Figure S4.

The lifetime of the propane gas HP state is on the time scale of seconds.[21] Moreover, the GRE phantom imaging also reveals fast polarization decay (as seen from the decrease of the SNR values—note the image intensity is scaled individually), likely also in part due to depolarizing effects of the RF pulses. Thus, we have investigated the feasibility of echo-planar imaging (EPI), in which one excitation RF pulse is employed to record an entire 2D slice. Figure 4c and Figure S5 show the utility of using slice-selective 20° RF excitation followed by ultra-fast image readout, allowing us to record eight slices of HP propane gas phantom in 0.40 s. Three representative 10-mm thick slices are shown in Figure 4c, revealing a hole in one of the images due to presence of the 1/8” OD Teflon line inside the phantom. Moreover, the EPI images also reveal a more pronounced (compared to GRE images discussed above) “ghost” artifact, which is likely due to the fact that imaging is performed with two HP resonances of the opposite sign—this notion is additionally supported by near perfect signal cancelation in two areas: below the “ghost” and below the sphere—likely due to signal cancellation due to image encoding of these two resonances of the opposite phase, *i.e.*, H_A and H_B in Figure 2d. This is not necessarily a limitation of this approach as a number of approaches have been developed for rephasing of the anti-phase resonances of HP propane gas.[33, 45] The recorded EPI images also demonstrate a remarkably high SNR of up to 1595. Even when accounting for larger voxels (approximately 10.6 times greater than the voxel size in GRE images in Figure 4b), the SNR of EPI images (per unit volume) was approximately four times higher than that of GRE images—at the same time the temporal resolution of EPI imaging was approximately 16 times higher than that of GRE imaging.

Pilot imaging of HP propane gas in excised pig lungs using a 0.35 T clinical MRI scanner.

We have also investigated the feasibility of pilot imaging of HP propane gas in the excised pig lungs, Figure 5. The overall experimental setup (Figure 5e) for these studies was similar to the one of 3 T imaging studies with the exception that the exhaust of the reactor was connected to the lung trachea via plastic tubing (Figure 5f), and thus the imaging of gas was performed at a physiologically relevant total pressure of 1 bar. Moreover, since the excised pig lungs contains tissue water, there is a substantial proton background signal. For example, thermally polarized images of inflated pig lungs (with propane or nitrogen) revealed a substantial anatomical signal in axial and coronal projections, Figure 5b and Figure 5d respectively. As a result, we have employed a background signal subtraction method[46]—the detailed description of the image processing is provided in the SI. A series of 2D slice-selective images was recorded during 5–6-s-long injection of HP propane gas in the

excised pig lungs with temporal resolution of 0.94 s. High-quality HP images were obtained from at least five images in each HP propane gas injection time series of the dynamic run. Representative axial and coronal images from each series are shown as color overlay (HP propane gas) over grayscale anatomical images in Figure 5a and Figure 5c respectively. The complete corresponding time series are presented in Figure S6 and Figure S8 respectively. The SNR(max) was 22 and 17 for axial and coronal scans, respectively.

MRI imaging with HP propane gas was reproducible. Indeed, a replicate HP propane gas injection study in the axial position (Figure S10) revealed similar intensity distribution as in the first axial dynamic run (Figure S6). Importantly, the replicate run was performed using refilling of the same gas-mixture storage can with fresh gas mixture using the same reactor. The scan-to-scan time duration was approximately 5 min, clearly demonstrating that the hyperpolarizer can be reused and provides reproducible results with fast polarizer reloading speed.

When the HP gas injection was completed, the HP gas signal experienced a fast decay due to T_1 relaxation and also due to the depolarizing effect of the RF pulses. The “effective” T_1 constant was measured to be 0.67 ± 0.40 s (Figure S6), 0.68 ± 0.39 s (Figure S8), and 0.64 ± 0.47 s (Figure S10), additionally highlighting the reproducibility albeit with large T_1 error bars. While this “effective” T_1 is rather short, the feasibility of HP propane imaging in physiologically relevant conditions in a clinical MRI scanner is clearly demonstrated in this pilot study. We also note that the detection sensitivity of this study likely has suffered substantially from the slow rate of HP propane gas injection—indeed, the bulk of injected HP gas (estimated at 0.6–0.7 sL) experienced depolarization (due to relaxation and RF pulsing) as it was injected during 5–6 s, while the “effective” relaxation constant is only 0.67 ± 0.40 s. Faster HP propane gas production and administration is envisioned to substantially improve the sensitivity of this scan—potentially by several fold.

Additional control experiments were also performed with injection of inert compressed nitrogen gas, which has no protons. The corresponding color-overlay axial and coronal studies revealed substantially attenuated signal in Figures S7, S11 and S9 respectively. The greatly reduced signal intensities in these control experiments are likely due to tissue expansion during gas injection.

Taken together, these pilot 0.35 T studies in excised pig lungs demonstrate the feasibility of reproducible high-quality ventilation imaging of the lung using HP propane gas despite the relatively short lifetime of HP state. The lifetime of the HP state of propane gas exhibits a nearly linear dependence on pressure with T_1 of ~1 s, and T_S of ~3 s, at 1 bar (total pressure) because of the spin-rotation relaxation mechanism, which is known to dominate for gases.[21, 47] It should be also emphasized that a number of potential improvements can be possibly envisioned to further increase the detection sensitivity, temporal and spatial resolution of such scans – active ongoing studies in our partnering laboratories. Although deuteration is unlikely to increase T_1 and T_S values for HP propane gas,[21, 48] the use of lower magnetic fields (*i.e.*, with B_0 < 0.35 T, where the long-lived spin states (LLSS) of HP propane exist, and undergo relaxation according to T_S versus T_1[31]) may be of practical benefit to extend the useful lifetime of the HP propane gas contrast agent.[49] Indeed, new low-field MRI

scanners are emerging, including the point-of-care Hyperfine MRI scanner[50] operating at 0.064 T, where LLSS are expected to exist for HP propane.[31]

Future studies and biomedical outlook.

While the produced HP state of propane gas lasts only for seconds, the possibility of a multi-day time window for storage and transportation of this hand-held ultra-low-cost device can be potentially transformative for potential application in the area of pulmonary imaging because it becomes possible to prepare the device in one location, while utilization can be performed substantially later at the potentially distant imaging suite (elsewhere). Since the device is portable and disposable, virtually no infrastructure investment is required for production, supplies storage, or utilization. Indeed, we envision that our propane hyperpolarizer can be potentially deployed as a disposable kit in the future, and further work in this field is currently ongoing in our labs. The future device can potentially benefit from a number of further improvements, including increasing the lifetime of storage as discussed above, improving the percentage polarization of produced propane gas,[51] more integrated design of the kit, etc.

While future studies should address safety of MRI with inhalable HP propane gas (including the study of excipients), it should be mentioned that FDA and other regulatory agencies are regulating propane as generally regarded as safe (GRAS[52]). Propane is a non-toxic asphyxiating gas (*i.e.* it is biochemically inert when administered *in vivo*; moreover, it has no observed developmental or systemic effects even under high (10000 ppm) concentration as studied in a randomized 90-day inhalation toxicity study).[53] Propane has widespread application in cosmetics, foods (FDA-approved foods propellant more broadly labeled as E944 food additive), and other biocompatible uses.[54] The highest dose administered to humans to date was 20% propane:air mixture by volume for a duration of 1 minute.[55–56] Based on the dosing principle of a single dose (~0.6–0.7 sL inhalation versus 20% for one minute) and the ultrafast imaging time, we expect that the intoxicating effect of a single 0.6–0.7 sL dose will be significantly less than that of 20% propane:air for one minute. Multiple inhalations/continuous feed of HP propane gas can also be envisioned, albeit at lower inhalation doses. However, the reader is reminded that HP propane gas has no current regulatory approval for MRI applications, and it may take several years to receive one. Despite the overall low toxicity of propane gas, possible side effects of a future HP propane lung MRI scan would certainly need to be explored as propane can potentially cause cardiac sensitization and CNS depression in volunteer exposure of 2 mins and longer.[57]

In the assessment of lung function, HP propane gas contrast agent can potentially offer a number of critical advantages over current HP ^{129}Xe technology (which has been recently approved by the FDA), including virtually no cost and space requirement of the needed infrastructure to produce HP gas contrast agent. Our hyperpolarizer can additionally be readily disposed of or recycled. Moreover, conventional clinical MRI scanners can be readily employed for imaging of HP propane gas without any scanner modifications or upgrades.

CONCLUSION

We have demonstrated that pure p-H_2 gas or p-H_2:propylene gas mixtures can be successfully loaded in commercial pressurized aluminum cans, where the gases can be stored for days without substantial loss of potency for producing HP states. Specifically, the T_S decay of pure p-H_2 gas was demonstrated to be up to 6.4 ± 1.3 days in disposable aluminum storage cans. Similarly, the decay of p-H_2 in the p-H_2:propylene gas mixtures gave a T_1 value of 6.0 ± 0.5 days. These relatively long lifetimes of the gas mixture potency allow for temporary storage and transportation of the hyperpolarizer, which was demonstrated in the example of gas mixture storage for approximately 4 hours before utilization for phantom imaging studies using a clinical 3 T MRI scanner without any modifications to the scanner hardware or pulse sequences. The propane hyperpolarizer delivers polarization value of up to 1.2% for each of the two HP resonances, and the device showed robust operation with respect to the gas flow rate, flow duration, and gas pressure. The device's robust performance enabled reproducible ventilation imaging of accessible air space in excised pig lungs, which was successfully demonstrated here for the first time for any proton-hyperpolarized sensing gas. Taken together, our propane hyperpolarizer can produce HP propane sensing gas on demand, which has been extensively validated by high-resolution NMR spectroscopy studies, phantom imaging 3 T MRI studies, and 0.35 T imaging studies in excised pig lungs. Although the hyperpolarizer tests in excised lungs cannot substitute for functional lung MRI scan in live animals (note that the pressure and dosing of the HP propane gas used here is expected to be similar as what would be used in such envisioned live-animal studies), the developments reported here bode well for a wide range of envisioned biomedical and clinical applications including near-future studies in live animals.

Supplementary Material

Refer to Web version on PubMed Central for supplementary material.

ACKNOWLEDGMENT

This work was supported by DOD CDMRP W81XWH-20-10576, W81XWH-20-10578, NSF CHE-1905341 and CHE-1904780, NHLBI R21HL154032, and NHLBI 1F32HL160108. O.G.S. and I.V.K. acknowledge financial support of this research by the Ministry of Science and Higher Education of the Russian Federation (grant no. 075-15-2020-779).

EYC and BMG declare a stake of ownership in XeUS Technologies LTD. EYC serves on the Scientific Advisory Board (SAB) and declares a stake of ownership in Vizma Life Sciences.

REFERENCES

1. Goodson BM; Whiting N; Coffey AM; Nikolaou P; Shi F; Gust BM; Gemeinhardt ME; Shchepin RV; Skinner JG; Birchall JR, et al. Hyperpolarization Methods for MRS. Emagres 2015, 4 (4), 797–810.
2. Nikolaou P; Goodson BM; Chekmenev EY NMR Hyperpolarization Techniques for Biomedicine. Chem. Eur. J 2015, 21 (8), 3156–3166. [PubMed: 25470566]
3. Goodson BM Nuclear magnetic resonance of laser-polarized noble gases in molecules, materials, and organisms. J. Magn. Reson 2002, 155 (2), 157–216. [PubMed: 12036331]

4. Eills J; Budker D; Cavagnero S; Chekmenev EY; Elliott SJ; Jannin S; Lesage A; Matysik J; Meersmann T; Prisner T, et al. Spin Hyperpolarization in Modern Magnetic Resonance. Chem. Rev 2023, 123 (4), 1417–1551. [PubMed: 36701528]
5. Albert MS; Cates GD; Driehuys B; Happer W; Saam B; Springer CS; Wishnia A. Biological Magnetic-Resonance-Imaging Using Laser Polarized Xe-129. Nature 1994, 370 (6486), 199–201. [PubMed: 8028666]
6. Hövener J-B; Pravdivtsev AN; Kidd B; Bowers CR; Glöggler S; Kovtunov KV; Plaumann M; Katz-Brull R; Buckenmaier K; Jerschow A, et al. Parahydrogen-based Hyperpolarization for Biomedicine. Angew. Chem. Int. Ed 2018, 57 (35), 11140–11162.
7. Barskiy DA; Coffey AM; Nikolaou P; Mikhaylov DM; Goodson BM; Branca RT; Lu GJ; Shapiro MG; Telkki V-V; Zhivonitko VV, et al. NMR Hyperpolarization Techniques of Gases. Chem. Eur. J 2017, 23 (4), 725–751. [PubMed: 27711999]
8. Kovtunov KV; Pokochueva EV; Salnikov OG; Cousin S; Kurzbach D; Vuichoud B; Jannin S; Chekmenev EY; Goodson BM; Barskiy DA, et al. Hyperpolarized NMR: d-DNP, PHIP, and SABRE. Chem. Asian J 2018, 13 (15), 1857–1871.
9. Mugler JP; Altes TA Hyperpolarized ^{129}Xe MRI of the human lung. J. Magn. Reson. Imaging 2013, 37 (2), 313–331. [PubMed: 23355432]
10. Walkup LL; Woods JC Translational applications of hyperpolarized ^{3}He and ^{129}Xe. NMR Biomed. 2014, 27 (12), 1429–1438. [PubMed: 24953709]
11. Khan AS; Harvey RL; Birchall JR; Irwin RK; Nikolaou P; Schrank G; Emami K; Dummer A; Barlow MJ; Goodson BM, et al. Enabling Clinical Technologies for Hyperpolarized Xenon-129 MRI and Spectroscopy. Angew. Chem. Int. Ed 2021, 60 (41), 22126–22147.
12. Bhaskar ND; Happer W; McClelland T. Efficiency of Spin Exchange Between Rubidium Spins And Xe-129 Nuclei In a Gas. Phys. Rev. Lett 1982, 49 (1), 25–28.
13. Kaushik SS; Cleveland ZI; Cofer GP; Metz G; Beaver D; Nouls J; Kraft M; Auffermann W; Wolber J; McAdams HP, et al. Diffusion-Weighted Hyperpolarized Xe-129 MRI in Healthy Volunteers and Subjects With Chronic Obstructive Pulmonary Disease. Magn. Reson. Med 2011, 65 (4), 1155–1165.
14. Stephen MJ; Emami K; Woodburn JM; Chia E; Kadlecek S; Zhu J; Pickup S; Ishii M; Rizi RR; Rossman M. Quantitative Assessment of Lung Ventilation and Microstructure in an Animal Model of Idiopathic Pulmonary Fibrosis Using Hyperpolarized Gas MRI. Acad. Radiol 2010, 17 (11), 1433–1443. [PubMed: 20934126]
15. Walker TG; Happer W. Spin-exchange optical pumping of noble-gas nuclei. Rev. Mod. Phys 1997, 69 (2), 629–642.
16. Zook AL; Adhyaru BB; Bowers CR High capacity production of > 65% spin polarized xenon-129 for NMR spectroscopy and imaging. J. Magn. Reson 2002, 159 (2), 175–182. [PubMed: 12482697]
17. Walker TG Fundamentals of Spin-Exchange Optical Pumping. J. Phys. Conf. Ser 2011, 294, 012001.
18. Rosen MS; Chupp TE; Coulter KP; Welsh RC; Swanson SD Polarized Xe-129 optical pumping/ spin exchange and delivery system for magnetic resonance spectroscopy and imaging studies. Rev. Sci. Instrum 1999, 70 (2), 1546–1552.
19. Nikolaou P; Coffey AM; Walkup LL; Gust BM; Whiting N; Newton H; Barcus S; Muradyan I; Dabaghyan M; Moroz GD, et al. Near-unity nuclear polarization with an 'open-source' 129Xe hyperpolarizer for NMR and MRI. Proc. Natl. Acad. Sci. U. S. A 2013, 110 (35), 14150–14155. [PubMed: 23946420]
20. Khan ASH,RL; Birchall JR; Irwin RK; Nikolaou P; Schrank G; Emami K; Dummer A; Barlow MJ; Goodson BM, et al. Enabling Clinical Technologies for Hyperpolarized Xenon-129 MRI and Spectroscopy. Angew. Chem. Int. Ed 2021, 60 (41), 22126–22147.
21. Ariyasingha NM; Salnikov OG; Kovtunov KV; Kovtunova LM; Bukhtiyarov VI; Goodson BM; Rosen MS; Koptyug IV; Gelovani JG; Chekmenev EY Relaxation Dynamics of Nuclear Long-Lived Spin States in Propane and Propane-d6 Hyperpolarized by Parahydrogen. J. Phys. Chem C 2019, 18 (123), 11734–11744.

22. Birchall JR; Irwin RK; Nikolaou P; Coffey AM; Kidd BE; Murphy M; Molway M; Bales LB; Ranta K; Barlow MJ, et al. XeUS: A second-generation automated open-source batch-mode clinical-scale hyperpolarizer. J. Magn. Reson 2020, 319, 106813.
23. Schroder L. Xenon for NMR biosensing - Inert but alert. Phys. Medica 2013, 29 (1), 3–16.
24. Chen RYZ; Fan FC; Kim S; Jan KM; Usami S; Chien S. Tissue-blood partition coefficient for xenon: temperature and hematocrit dependence. J. Appl. Physiol 1980, 49 (2), 178–183. [PubMed: 7400000]
25. Meloni EG; Gillis TE; Manoukian J; Kaufman MJ Xenon Impairs Reconsolidation of Fear Memories in a Rat Model of Post-Traumatic Stress Disorder (PTSD). PLoS One 2014, 9 (8), e106189.
26. Bouchard LS; Kovtunov KV; Burt SR; Anwar MS; Koptyug IV; Sagdeev RZ; Pines A. Para-hydrogen-enhanced hyperpolarized gas-phase magnetic resonance imaging. Angew. Chem. Int. Ed 2007, 46 (22), 4064–4068.
27. Bouchard LS; Burt SR; Anwar MS; Kovtunov KV; Koptyug IV; Pines A. NMR imaging of catalytic hydrogenation in microreactors with the use of para-hydrogen. Science 2008, 319 (5862), 442–445. [PubMed: 18218891]
28. Kovtunov KV; Barskiy DA; Coffey AM; Truong ML; Salnikov OG; Khudorozhkov AK; Inozemtseva EA; Prosvirin IP; Bukhtiyarov VI; Waddell KW, et al. High-resolution 3D Proton Hyperpolarized Gas MRI Enabled by Parahydrogen and Rh/TiO2 Heterogeneous Catalyst. Chem. Eur. J 2014, 20 (37), 11636–11639. [PubMed: 24961814]
29. Kovtunov KV; Romanov AS; Salnikov OG; Barskiy DA; Chekmenev EY; Koptyug IV Gas Phase UTE MRI of Propane and Propene. Tomography 2016, 2 (1), 49–55. [PubMed: 27478870]
30. Ariyasingha NM; Joalland B; Younes HR; Salnikov OG; Chukanov NV; Kovtunov KV; Kovtunova LM; Bukhtiyarov VI; Koptyug IV; Gelovani JG, et al. Parahydrogen-Induced Polarization of Diethyl Ether Anesthetic. Chem. Eur. J 2020, 26, 13621–13626. [PubMed: 32667687]
31. Barskiy DA; Salnikov OG; Romanov AS; Feldman MA; Coffey AM; Kovtunov KV; Koptyug IV; Chekmenev EY NMR Spin-Lock Induced Crossing (SLIC) Dispersion and Long-Lived Spin States of Gaseous Propane at Low Magnetic Field (0.05 T). J. Magn. Reson 2017, 276, 78–85. [PubMed: 28152435]
32. Salnikov OG; Nikolaou P; Ariyasingha NM; Kovtunov KV; Koptyug IV; Chekmenev EY Clinical-Scale Batch-Mode Production of Hyperpolarized Propane Gas for MRI. Anal. Chem 2019, 91 (7), 4741–4746. [PubMed: 30855132]
33. Barskiy DA; Kovtunov KV; Gerasimov EY; Phipps MA; Salnikov OG; Coffey AM; Kovtunova LM; Prosvirin IP; Bukhtiyarov VI; Koptyug IV, et al. 2D Mapping of NMR Signal Enhancement and Relaxation for Heterogeneously Hyperpolarized Propane Gas. J. Phys. Chem. C 2017, 121 (18), 10038–10046.
34. Kovtunov KV; Zhivonitko VV; Skovpin IV; Barskiy DA; Koptyug IV Parahydrogen-induced polarization in heterogeneous catalytic processes. Top. Curr. Chem 2013, 338, 123–180. [PubMed: 23097028]
35. Bowers CR; Weitekamp DP Transformation of Symmetrization Order to Nuclear-Spin Magnetization by Chemical-Reaction and Nuclear-Magnetic-Resonance. Phys. Rev. Lett 1986, 57 (21), 2645–2648. [PubMed: 10033824]
36. Eisenschmid TC; Kirss RU; Deutsch PP; Hommeltoft SI; Eisenberg R; Bargon J; Lawler RG; Balch AL Para Hydrogen Induced Polarization In Hydrogenation Reactions. J. Am. Chem. Soc 1987, 109 (26), 8089–8091.
37. Birchall JR; Coffey AM; Goodson BM; Chekmenev EY High-Pressure Clinical-Scale 87% Parahydrogen Generator. Anal. Chem 2020, 92 (23), 15280–15284. [PubMed: 33170640]
38. Nantogma S; Joalland B; Wilkens K; Chekmenev , E. Y. Clinical-Scale Production of Nearly Pure (>98.5%) Parahydrogen and Quantification by Benchtop NMR Spectroscopy. Anal. Chem 2021, 93 (7), 3594–3601. [PubMed: 33539068]
39. Hoult DI; Richards RE The signal-to-noise ratio of the nuclear magnetic resonance experiment. J. Magn. Reson 1976, 24 (1), 71–85.

40. Kovtunov KV; Koptyug IV; Fekete M; Duckett SB; Theis T; Joalland B; Chekmenev EY Parahydrogen-induced Hyperpolarization of Gases. Angew. Chem. Int. Ed 2020, 59 (41), 17788–17797.
41. Feng B; Coffey AM; Colon RD; Chekmenev EY; Waddell KW A pulsed injection parahydrogen generator and techniques for quantifying enrichment. J. Magn. Reson 2012, 214, 258–262. [PubMed: 22188975]
42. Dwyer AJ; Knop RH; Hoult DI Frequency shift artifacts in MR imaging. J. Comput. Assist. Tomogr 1985, 9 (1), 16–8. [PubMed: 3968259]
43. Babcock EE; Brateman L; Weinreb JC; Horner SD; Nunnally RL Edge artifacts in MR images: chemical shift effect. J. Comput. Assist. Tomogr 1985, 9 (2), 252–7. [PubMed: 3973146]
44. Hood MN; Ho VB; Smirniotopoulos JG; Szumowski J. Chemical shift: the artifact and clinical tool revisited. Radiographics 1999, 19 (2), 357–71. [PubMed: 10194784]
45. Kononenko ES; Svyatova AI; Skovpin IV; Kovtunova LM; Gerasimov EY; Koptyug IV Getting the Most out of Parahydrogen-Induced Signal Enhancement for MRI of Reacting Heterogeneous Systems. J. Phys. Chem. C 2022, 126 (35), 14914–14921.
46. Kopanski A; Hane F; Li T; Albert M, 1H Magnetic Resonance Imaging of the Lungs Using Propane As An Inhalation Agent. In 25th ISMRM Conference, April 22–27, Honolulu, Hawaii, 2017; p 2162.
47. McClung RED, Spin–Rotation Relaxation Theory. In eMagRes, 2007; 10.1002/9780470034590.emrstm0524.
48. Kovtunov KV; Truong ML; Barskiy DA; Salnikov OG; Bukhtiyarov VI; Coffey AM; Waddell KW; Koptyug IV; Chekmenev EY Propane-d6 Heterogeneously Hyperpolarized by Parahydrogen. J. Phys. Chem. C 2014, 118 (48), 28234–28243.
49. Kovtunov KV; Truong ML; Barskiy DA; Koptyug IV; Coffey AM; Waddell KW; Chekmenev EY Long-lived Spin States for Low-field Hyperpolarized Gas MRI. Chem. Eur. J 2014, 20 (45), 14629–14632. [PubMed: 25263795]
50. Iglesias JE; Schleicher R; Laguna S; Billot B; Schaefer P; McKaig B; Goldstein JN; Sheth KN; Rosen MS; Kimberly WT Quantitative Brain Morphometry of Portable Low-Field-Strength MRI Using Super-Resolution Machine Learning. Radiology 2023, 306 (3), e220522.
51. Zhao EW; Maligal-Ganesh R; Xiao C; Goh T-W; Qi Z; Pei Y; Hagelin-Weaver HE; Huang W; Bowers CR Silica-Encapsulated Pt-Sn Intermetallic Nanoparticles: A Robust Catalytic Platform for Parahydrogen-Induced Polarization of Gases and Liquids. Angew. Chem. Int. Ed 2017, 56 (14), 3925–3929.
52. Burdock GA; Carabin IG Generally recognized as safe (GRAS): history and description. Toxicol. Lett 2004, 150 (1), 3–18. [PubMed: 15068820]
53. McKee RH; Herron D; Saperstein M; Podhasky P; Hoffman GM; Roberts L. The Toxicological Properties of Petroleum Gases. Int. J. Toxicol 2014, 33, 28S–51S. [PubMed: 24179026]
54. Hijazi R; Taylor D; Richardson J. Effect of topical alkane vapocoolant spray on pain with intravenous cannulation in patients in emergency departments: randomised double blind placebo controlled trial. Br. Med. J 2009, 338, 5.
55. National Research Council, Acute Exposure Guideline Levels for Selected Airborne Chemicals: Volume 12. The National Academies Press: Washington, DC, 2012; p 334.
56. Reinhardt CF; Azar A; Maxfield ME; Smith PE; Mullin LS Cardiac Arrhythmias and Aerosol “Sniffing”. Archives of Environmental Health: An International Journal 1971, 22 (2), 265–279.
57. Committee on Acute Exposure Guideline, Levels Committee on, Toxicology Board on Environmental, Studies Toxicology, Division on, Earth Life, Studies, National Research, Council. In Acute Exposure Guideline Levels for Selected Airborne Chemicals: Volume 12, National Academies Press (US): Washington (DC), 2012.

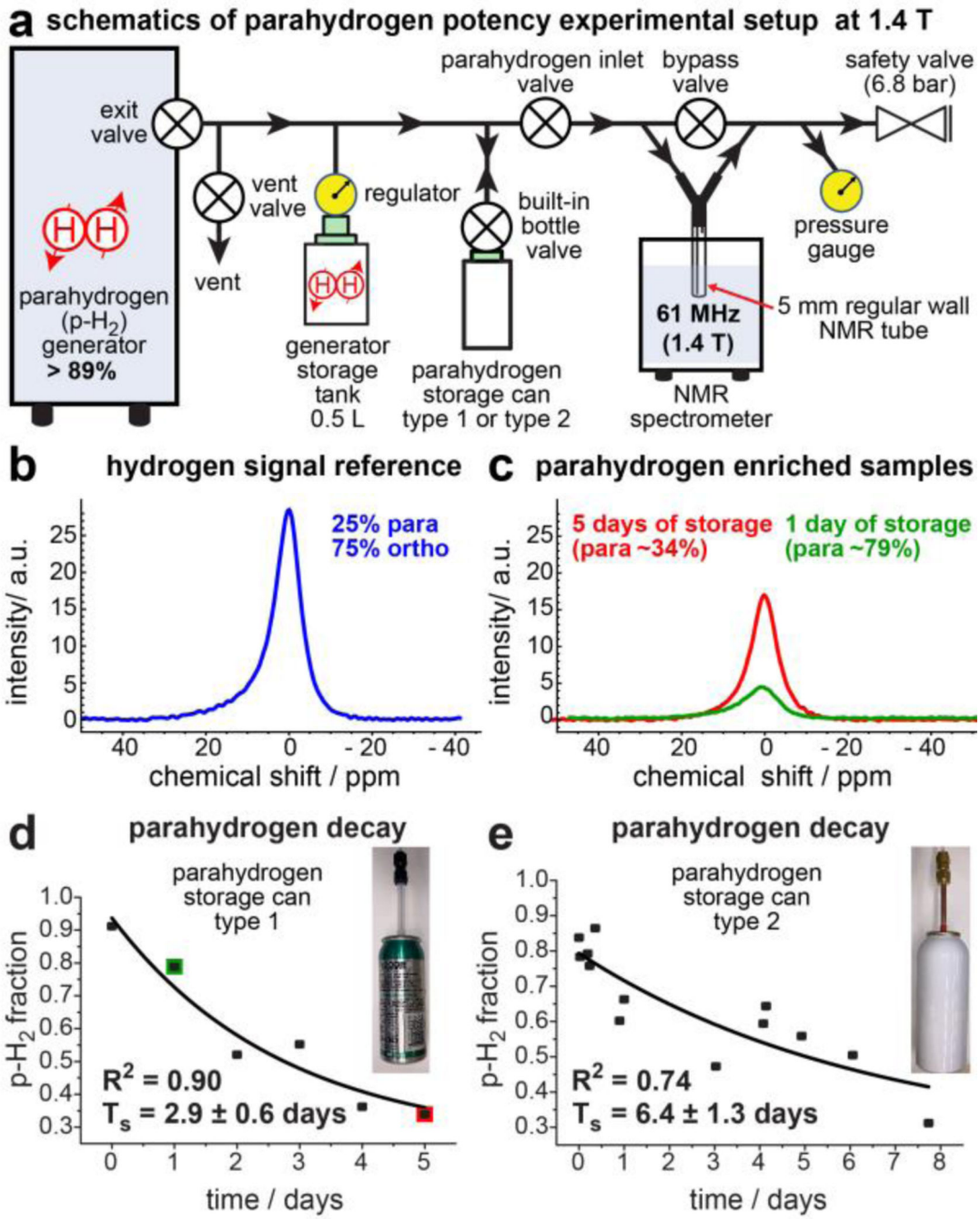

Figure 1.

The study of p-H_2 gas storage in disposable aluminum cans. a) Schematic diagram of the experimental setup whereby a parahydrogen generator is used to fill aluminum p-H_2 storage cans. b) ^{1}H NMR spectrum of normal hydrogen gas signal reference consisting of 75% orthohydrogen (o-H_2) and 25% p-H_2. c) ^{1}H NMR spectra of the p-H_2 enriched samples collected after different storage durations in an aluminum can (type 1). Green and red spectral traces correspond to the spectra collected after 1 day of and 5 days of p-H_2 gas

storage with p-H_2 fractions of ~79% and ~34% respectively. d,e) Decay plots for p-H_2 gas back-conversion to o-H_2 in bottle types 1 (d) and 2 (e).

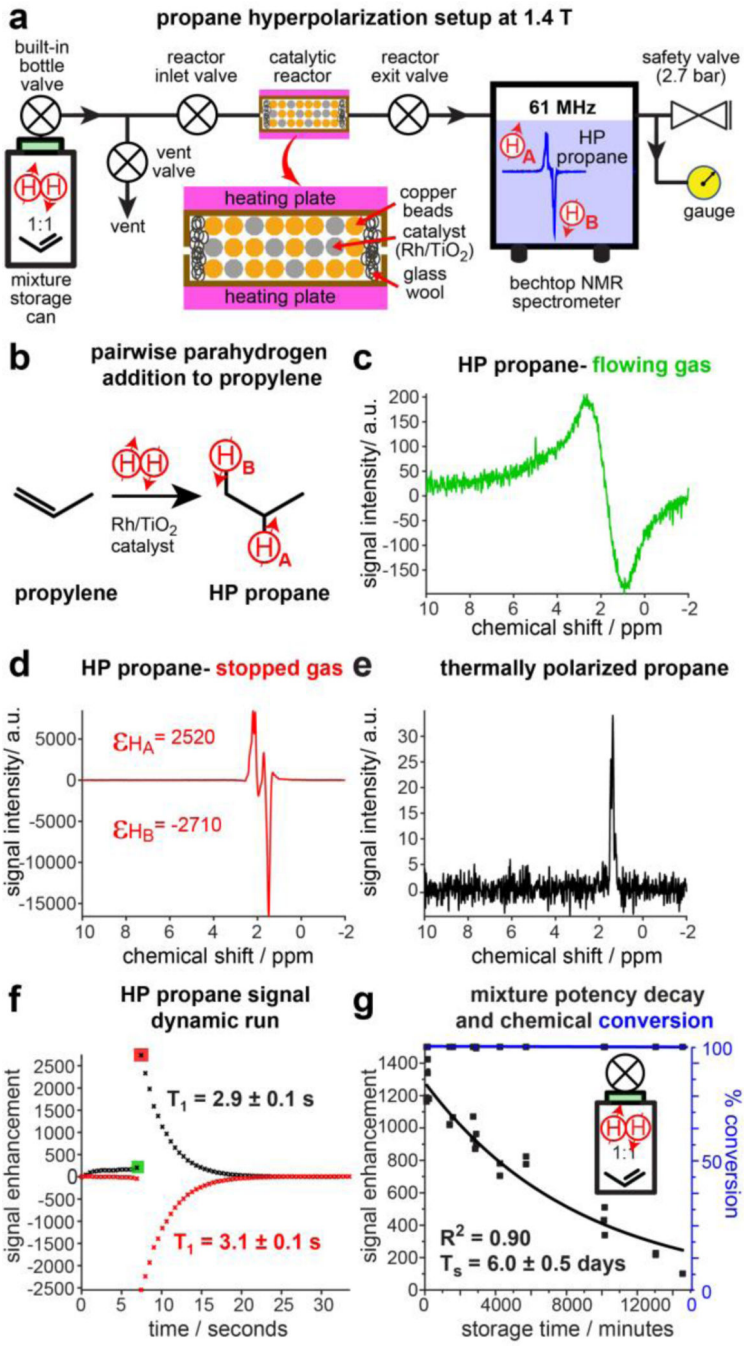

Figure 2.

a) Schematic diagram of the experimental setup for the production of HP propane and its detection at 1.4 T. An inset diagram of the catalytic reactor shows the catalyst particles and copper beads mixed inside of the reactor. b) Schematic of the PHIP process comprising pairwise addition of p-H_2 to propylene forming HP propane gas. c) ^{1}H NMR spectrum of continuously flowing HP propane gas at 1.4 T. d) ^{1}H NMR spectrum of stopped-flow HP propane gas at 1.4 T. e) Corresponding ^{1}H NMR spectrum (employed for signal referencing) of thermally polarized stopped-flow propane gas. Note the signal intensity scale employs

the same a.u. scale for all data shown in displays c-e. f) Representative pseudo-2D NMR experiment showing the T_1 decay of HP propane signal enhancement after HP gas was stopped after ~7 s of continuous gas flow (the color coded squares denote the data points for which spectra are shown in displays c (green) and d (red), respectively. g) The dependence of the ^{1}H NMR signal enhancement of stopped-flow HP propane gas on the storage time of the p-H_2:propylene gas mixture in the type 2 storage can (black) and the dependence of chemical conversion of propylene to propane on the storage time of the p-H_2:propylene gas mixture (blue). The data was recorded using 3.7 bar total pressure and 7.5 sLm flow rate.

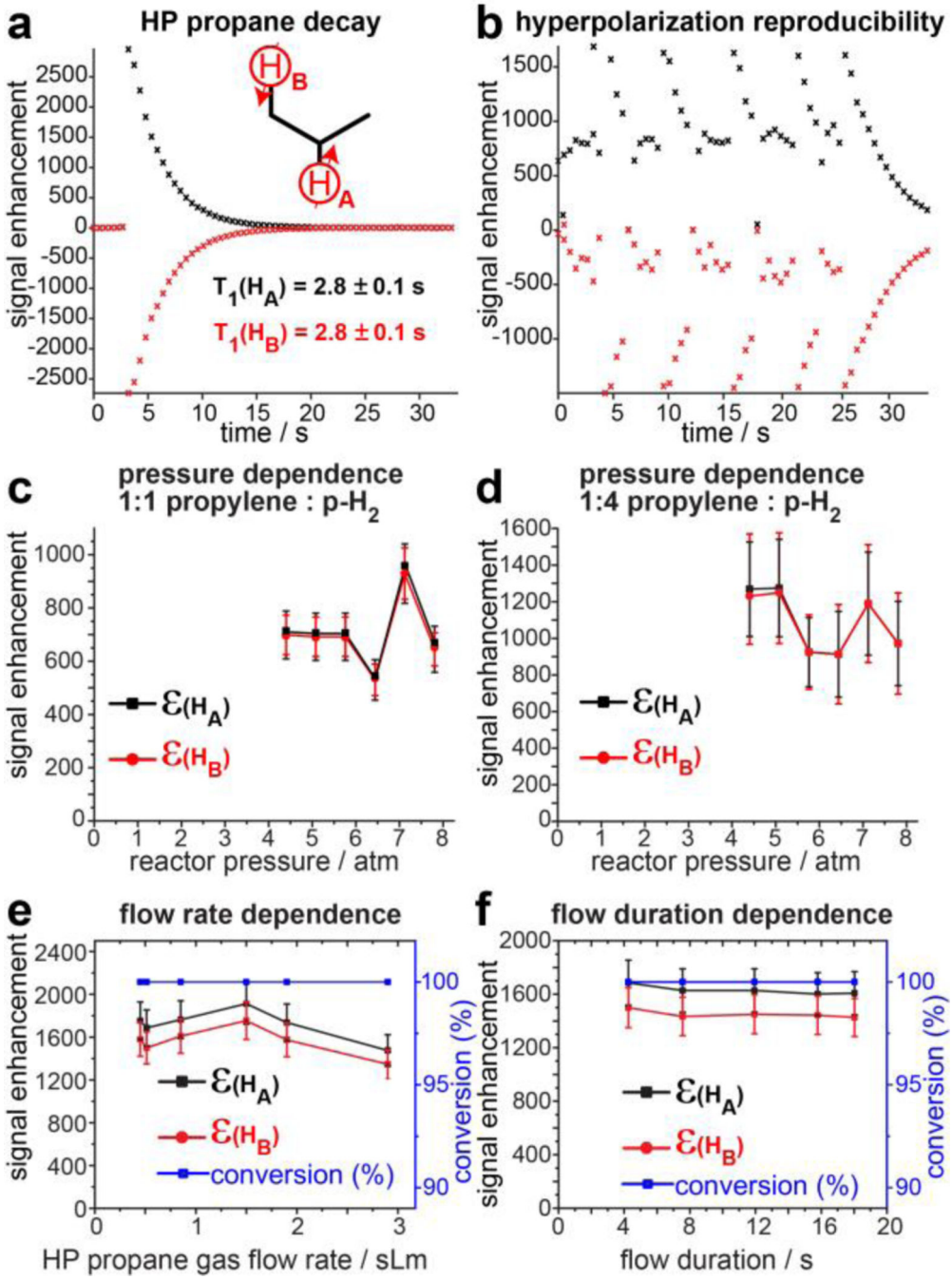

Figure 3.

PHIP studies of HP propane reactor robustness via spectroscopic detection using a 1.4 T NMR spectrometer. a) Representative pseudo-2D NMR experiment showing the T_1 decay of HP propane signal enhancement after HP gas was stopped at ~3 s. b) Representative pseudo-2D NMR experiment, where the flow of HP propane gas was repeatedly (5 repeats) stopped for ~3 s and then restarted for ~3 s. c) The dependence of ε_H values of HP propane on reactor pressure with a 1:1 propylene:p-H_2 gas mixture. d) The dependence of ε_H values of HP propane on reactor pressure with a 1:4 propylene:p-H_2 gas mixture. e)

The dependence of ε_H values and propylene chemical conversion of HP propane on the gas flow rate. f) The dependence of ε_H values and propylene chemical conversion of HP propane on the gas flow rate duration. All experiments were performed at 3.7 bar total gas pressure, using 1:1 mixture of propylene:p-H_2, and 0.8 sLm HP propane gas flow rate unless otherwise noted. The results shown in display e were obtained using needle valve, and the results shown in all other displays were obtained using mass flow controller using the modified setup shown in Figure S3.

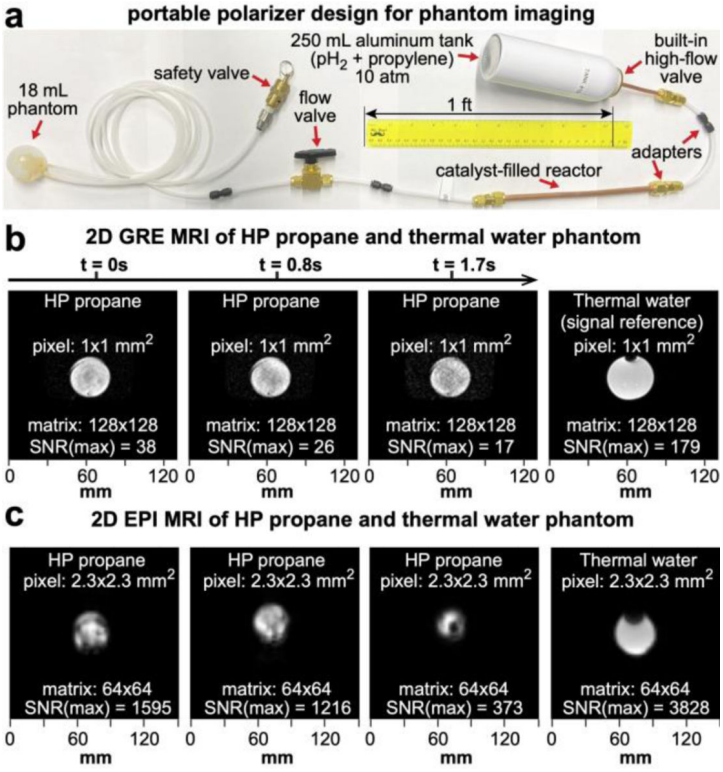

Figure 4.

Phantom validation studies of HP propane using a 3 T clinical MRI scanner. a) Schematics of the portable experimental polarizer design used for phantom validation studies. Premixed gas mixture in the storage can was delivered to the reactor by actuating the high flow valve. b) Time series of slice-selective (5-mm thick) 2D GRE images of HP propane-filled hollow-sphere phantom and the corresponding thermally-polarized water image acquired using a wrist RF coil; imaging parameters: 128×128 matrix, FOV=130×130 mm^2. c) 2D slices of EPI imaging (10-mm thick) of HP propane-filled hollow-sphere phantom and the corresponding thermally-polarized water image acquired using a wrist RF coil; imaging parameters: 64×64 matrix, FOV=150×150 mm^2; total scan time (8 slices) is 0.40 s (the right display shows the corresponding image from thermally polarized water phantom of the same geometry). Propane concentration was estimated at 0.13 M, and water concentration was 55 M.

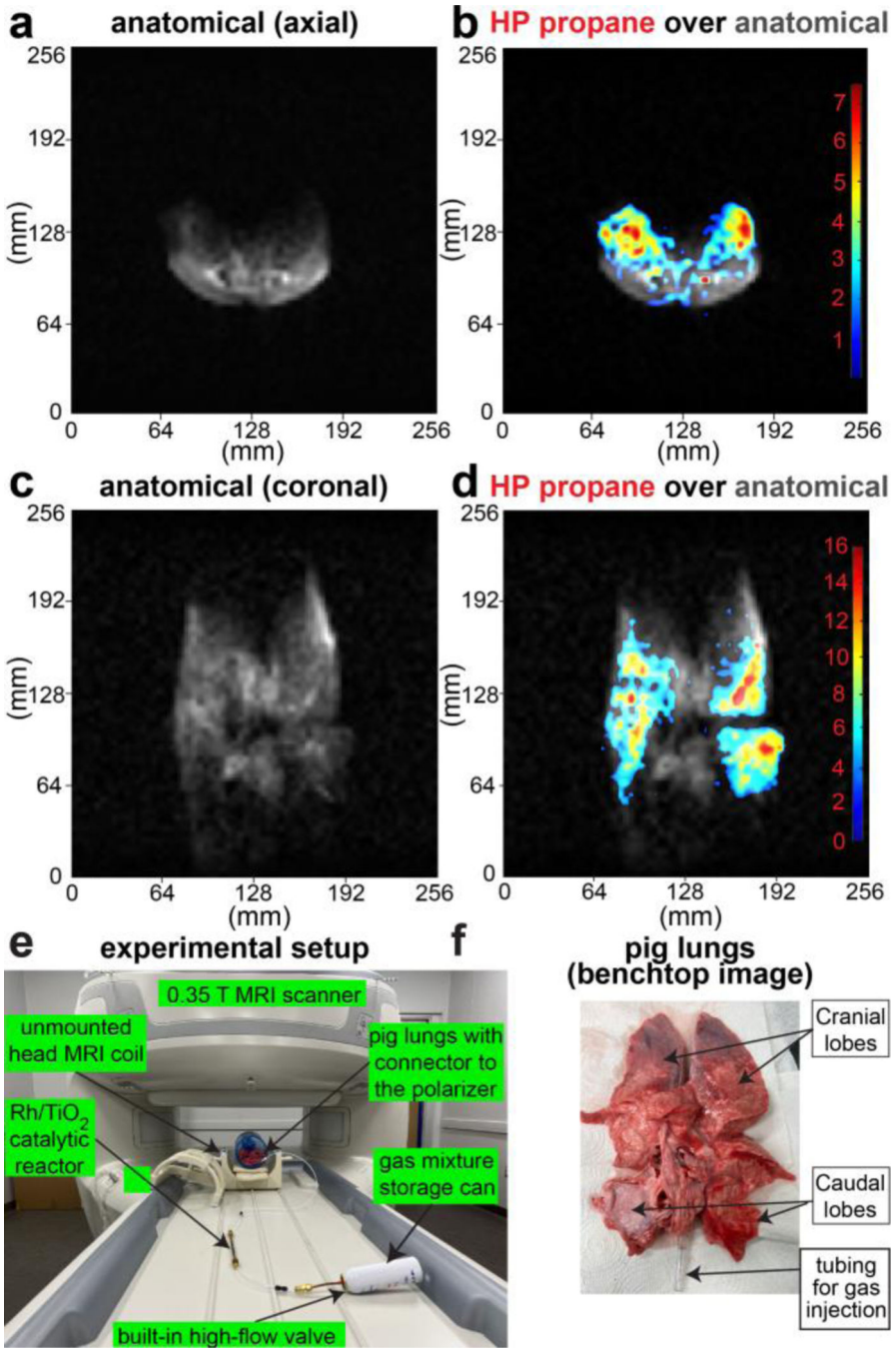

Figure 5.

Fast slice-selective 2D GRE images of HP propane gas injected in the excised pig lungs and recorded with 64×64 imaging matrix over 256×256 mm^2 FOV, 50-mm slice thickness, and 30-degree slice-selective RF pulse. a) Axial anatomical image of the inflated excised pig lung, b) Corresponding axial false-color image of HP propane gas contrast agent overlaid over greyscale axial anatomical image shown in display a, c) annotated photo of the experimental setup showing the gas mixture tank, Rh/TiO_2 reactor, unmounted head 0.35 T MRI coil and gas connection from the reactor outlet to the lungs' trachea. d) Coronal

anatomical image of the inflated excised pig lungs, e) Corresponding coronal false-color image of HP propane gas contrast agent overlaid over greyscale coronal anatomical image shown in display d. f) Annotated photo of the excised pig lungs employed for the pilot imaging studies. Each image in displays a, b, d, and e was acquired in 0.94 s, see SI for additional images and details.